Steel and Composite Structures, *Vol. 56, No. 6 (2025) 465-474*
https://doi.org/10.12989/scs.2025.56.6.465

Parametric analysis of transmission lines embedded in steel–concrete composite structures: A computational study

Dongsoo Lee[1a], Jong-Sub Lee[2b], Younghoon Lee[2c], Thomas H.-K. Kang[3b] and Jung-Doung Yu*[4]

[1]*Department of Civil and Environmental Engineering, University of Illinois Urbana-Champaign, 205 North Mathews, Urbana, IL 61801, USA*
[2]*School of Civil, Environmental and Architectural Engineering, Korea University, 145, Anam-ro, Seongbuk-gu, Seoul 02841, Republic of Korea*
[3]*Department of Architecture & Architectural Engineering, Seoul National University, 1 Gwanak-ro, Gwanak-gu, Seoul 08826, Republic of Korea*
[4]*Department of Civil Engineering, Jeonbuk National University, 567 Baekje-daero, Deokjin-gu, Jeonju-si, Jeollabuk-do, Republic of Korea*

(Received June 14, 2025, Revised July 7, 2025, Accepted July 8, 2025)

Abstract. This paper presents a parametric analysis of a two-conductor transmission line embedded in steel–concrete composite structures. The line configuration consists of a steel rebar and PVC-insulated copper wire, with spacing varied from near-contact (14.35 mm) to 3 m. The resistance, inductance, capacitance, conductance, and characteristic impedance of the transmission line are modeled considering skin effect, proximity effect, and frequency. The results show that resistance and conductance are strongly affected by both frequency and conductor spacing, whereas inductance and capacitance are primarily governed by geometry. Characteristic impedance exhibits a combined dependence on spacing and frequency, with significant increases observed at wide spacings and high frequencies. These findings provide valuable insights into the electromagnetic behavior of embedded transmission lines, with implications for structural health monitoring of steel–concrete composite structures.

Keywords: characteristic impedance; frequency-dependent RLGC; skin and proximity effects; steel–concrete composite; transmission line

1. Introduction

Remote sensing techniques based on electromagnetic waves have been increasingly applied in civil engineering. Ground-penetrating radar (GPR) is one of the most widely used ground-based methods for site investigations and assessing the condition of infrastructure. In addition, satellite and airborne remote sensing technologies, including synthetic aperture radar (SAR), terrestrial laser scanning (TLS), and unmanned aircraft systems (UAS), are now frequently used for monitoring ground subsidence and surface deformation (Becker *et al*. 2024, Nur *et al*. 2024, Park *et al*. 2024, Islam *et al*. 2025). Although these methods provide advantages such as rapid data collection and non-contact operation, they are also subject to several limitations, particularly in terms of penetration depth, environmental constraints, and the complexity of data processing and interpretation. A transmission line is a pair of conductors with a specific structure designed to stably transmit electromagnetic waves (Cole 1977, Kalaga and Yenumula 2016). Generally, a transmission line consists of two or more conductors used as signal and return paths (Lee *et al*. 2023b). Maintaining a constant impedance between the signal and return paths minimizes the energy loss of electromagnetic waves during their propagation along the transmission line (Bogatin 2004). Thus, studies on transmission lines in electrical engineering have focused on impedance matching to reduce energy losses (van Rensburg *et al*. 2014, Joseph *et al*. 2020). Time-domain reflectometry (TDR) is suggested to investigate the impedance variation at a specific point in transmission lines. TDR records the impedance with the travel time of electromagnetic waves, enabling the detection of impedance-mismatched points such as cable faults (Gnerlich 1989). Thus, the impedance of each point on the transmission lines can be evaluated using this technique, enabling the observation of signal integrity.

However, the lossy characteristics of transmission lines have been utilized for various purposes in civil engineering (Noborio 2001, Robinson *et al*. 2003, Lee *et al*. 2024b). Civil engineers have developed TDR probes by intentionally enlarging the space between transmission line conductors, thereby expanding the effective range of electromagnetic waves. For instance, TDR probes inserted into soils have been extensively used to estimate the soil moisture content (Davis and Annan 1977, Pastuszka *et al*. 2014, Lee *et al*. 2018, Park *et al*. 2023). Moreover, TDR has been implemented for monitoring slope stability (Farrington and Sargand 2006, Wahab *et al*. 2016, Kumar 2020). TDR sensors embedded in the ground capture deformation by identifying changes in impedance along coaxial cables, enabling continuous and remote monitoring for landslide early warning. (O'connor and Dowding 2021). Additionally,

*Corresponding author, Ph.D. Assistant Professor
E-mail: jungdoung@jbnu.ac.kr
[a]Ph.D. Postdoctoral Research Associate
[b]Ph.D. Professor
[c]Ph.D. Student

ISSN: 1229-9367 (Print), 1598-6233 (Online)

TDR techniques have been employed to identify cracks in concrete structures (Sun *et al*. 2009). Changes in impedance due to structural discontinuities or defects are captured by TDR sensors, enabling the early detection and proactive maintenance of civil infrastructure (Lin 2009). In addition, TDR-based techniques have been employed for detecting leakage in underground pipelines (Cataldo *et al*. 2016, Aghda *et al*. 2018). Leakage alters the dielectric properties of the surrounding soil due to fluid infiltration, leading to changes in the impedance measured by TDR sensors. This phenomenon provides a reliable and efficient means of identifying leaks (Cataldo *et al*. 2017).

The TDR technique has also been used for the structural health monitoring (SHM) in civil engineering (Yu *et al*. 2018, Lee and Yu 2019, Yu and Lee 2020, Yu *et al*. 2020a, Lee *et al*. 2023c, Lee *et al*. 2024a, Lee and Yu 2024). Continuous SHM over a wide area of a concrete structure has traditionally been challenging. A TDR-based SHM method called electromagnetic wave logging (EWL) has been proposed to overcome these limitations (Lee *et al*. 2018). EWL can simultaneously monitor long sections of structures using electrical wires embedded in concrete. To configure a transmission line within concrete, EWL uses an electrical wire as the signal path and another wire or rebar as the return path (Yu *et al*. 2020b). Furthermore, some studies have employed connectors to introduce artificial inflections into the TDR signal, enabling precise analysis (Lee *et al*. 2024c, Lee *et al*. 2024e). Evaluation of concrete quality through long-term monitoring of signals (Lee *et al*. 2023a, Lee *et al*. 2024d, Lee *et al*. 2025). Although extensive research has been conducted on these basic applications, studies investigating the effect of the transmission line configuration and its constituent components on signals remain limited.

The present study conducts a computational analysis to investigate the electromagnetic behavior of a transmission line. The theoretical framework focuses on four fundamental parameters of the transmission line, namely resistance, inductance, conductance, and capacitance, which are critical for determining the characteristic impedance. An analytical model is developed for a two-conductor transmission line composed of a reinforcing bar and an electrical wire. The interrelationships among the four primary transmission line parameters are examined with respect to conductor spacing and wave frequency. Furthermore, their effects on the characteristic impedance are thoroughly analyzed and discussed.

2. Theoretical background

2.1 Skin effect and resistance

Under alternating current (AC) excitation, the distribution of current within a conductor becomes non-uniform owing to the skin effect, wherein the current density is concentrated near the surface of the conductor. This effect causes the current to decay exponentially with depth from the surface. The characteristic depth at which the current density falls to $1/e$ (approximately 36.8%) of its surface value is referred to as the skin depth (or characteristic depth of penetration), denoted by δ (Pozar 2012). For a nonmagnetic conductor characterized by electrical conductivity σ (or resistivity $\rho = 1/\sigma$) and magnetic permeability μ, the skin depth at an angular frequency $\omega = 2\pi f$ is given by (Collin 2007, Pozar 2012)

$$\delta = \sqrt{\frac{2}{\omega\mu\sigma}} = \sqrt{\frac{2\rho}{\omega\mu}} \tag{1}$$

At sufficiently high frequencies ($\delta \ll a$, where a is the conductor radius), the AC resistance per unit length $R_{ac}(f)$ of a cylindrical conductor is approximated by (Collin 2007, Paul 2007, Pozar 2012)

$$R_{ac}(f) = \frac{R_s}{2\pi a} = \frac{\rho}{2\pi a\delta(f)} = \frac{\rho}{2\pi a}\sqrt{\frac{\omega\mu}{2\rho}} \propto \sqrt{f} \tag{2}$$

where R_s is the surface resistance per unit area, defined as ρ/δ.

When the skin depth δ becomes comparable to or exceeds the conductor radius a, as occurs at very low frequencies, a more rigorous expression involving Bessel functions is required to accurately compute the AC resistance (Pozar 2012). However, for the frequency range considered in this study (above 1 MHz), the condition $\delta \ll a$ holds true for conductors, even at frequencies as low as a few megahertz. Therefore, the simplified expressions given in Eq. (2) remain valid and provide sufficiently accurate estimates of the per-unit-length AC resistance.

2.2 Proximity effect

In addition to the skin effect, the proximity effect becomes significant when alternating currents in neighboring conductors induce magnetic fields that distort the current distribution in each conductor. In the case of two parallel cylindrical conductors carrying equal and opposite currents, as commonly observed in differential transmission line configurations, the magnetic field concentrated in the region between the conductors causes the current to crowd on the outer surfaces facing away from each other. This redistribution of current results in an increase in AC resistance beyond that predicted by the skin effect alone.

If conductors are closely spaced, the proximity effect causes the electrical charge to become non-uniform around the conductor peripheries. Specifically, charge distributions tend to be concentrated on the adjacent surfaces of the conductors (Paul 2007, Pozar 2012). Dowell (1966) derived the following proximity loss formula for cylindrical conductors:

$$K_R = Re\{\alpha h \cosh(\alpha h)\} + \frac{m^2 - 1}{3} Re\left\{2\alpha h \tanh\left(\frac{\alpha h}{2}\right)\right\} \tag{3}$$

where K_R is called the Dowell's factor, h is the conductor diameter, $m = 2$ is the number of conductors, and α is the complex propagation constant within the conductor, defined as

$$\alpha = \sqrt{j\omega\mu_0\sigma\eta} = (1+j)\sqrt{\frac{\omega\mu_0\sigma\eta}{2}} \tag{4}$$

where η denotes the porosity factor, which is assumed to be 1 for solid conductors.

The total AC resistance per unit length, $R(\omega)$, is the sum of the individual resistances of conductors. The AC resistance is calculated using Dowell's equation (Dowell 1966), which was originally developed to model eddy current losses in transformer windings and is now widely applied to calculate AC resistance in multi-conductor systems. It accounts for both the skin and proximity effects. The AC resistance of each conductor is given by:

$$R_{ac}(\omega) = R_{dc} \cdot K_R \tag{5}$$

where R_{dc} is the DC resistance per unit length.

2.3 Inductance

The total inductance per unit length, $L(\omega, D)$, is expressed as the sum of the external inductance (L_{ext}) and the frequency-dependent internal inductance (L_{int}):

$$L(\omega, D) = L_{ext}(D) + L_{int}(\omega) \tag{6}$$

Based on magnetostatic theory, the external inductance of a two-conductor transmission line can be determined by the geometry as follows (Grigsby 2007):

$$L_{ext}(D) = \frac{\mu_0}{\pi}\cosh^{-1}\left(\frac{D}{2 \cdot GMR}\right) \tag{7}$$

where GMR is the geometric mean radius of the conductors, defined as $GMR = \sqrt{a_1 + a_{2,}}$.

The internal inductance decreases with increasing frequency owing to the skin effect, which confines the current to a smaller area near the conductor surface (Paul 2007, Pozar 2012).

$$L_{int}(\omega) \approx \frac{\mu\delta}{4\pi a} = \frac{1}{4\pi a}\sqrt{\frac{2\mu\rho}{\omega}} \propto \frac{1}{\sqrt{f}} \tag{8}$$

2.4 Capacitance and conductance

Capacitance and conductance are determined by the geometry and dielectric properties of the surrounding medium. The frequency-dependent complex permittivity can be determined using the single-pole Debye relaxation model, which describes the response of dipolar polarization in a dielectric material to a changing electric field and is defined as (Debye 1913)

$$\hat{\varepsilon}_r(\omega) = \varepsilon_{r,\infty} + \frac{\varepsilon_{r,s} - \varepsilon_{r,\infty}}{1 + j\omega\tau} \tag{9}$$

where $\varepsilon_{r,s}$ is the effective static permittivity, $\varepsilon_{r,\infty}$ is the permittivity at infinite frequency, and τ is the relaxation time. Because the real part of the complex permittivity contributes to energy storage (i.e., capacitance), the capacitance per unit length, $C(\omega, D)$, for a two-conductor transmission line can be expressed as follows (Paul 2007, Pozar 2012):

$$C(\omega, D) = \frac{\pi\varepsilon_0 Re\{\hat{\varepsilon}_r(\omega)\}}{\cosh^{-1}(\frac{D}{2 \cdot GMR})} \tag{10}$$

Based on the telegrapher's equations, the conductance per unit length represents both the leakage (DC) and dielectric loss (AC) paths. At low frequencies, or when DC leakage current occurs owing to finite dielectric conductivity,

$$G_{dc}(D) = \sigma \cdot \frac{C_0(D)}{\varepsilon_0} \tag{11}$$

where $C_0(D)$ is the base capacitance per unit length without frequency dependency. Thus, Eq. (11) represents a purely resistive shunt path independent of the frequency. Real dielectric materials absorb energy under AC fields. This is captured by the loss tangent $\tan\delta(\omega)$, representing dielectric loss via loss tangent.

$$G_{dielectric}(\omega) = \omega C(\omega, D)\tan\delta(\omega) \tag{12}$$

The total conductance, $G(\omega, D)$, is derived by summing Eqs. (11) and (12), subsequently expressed in terms of complex permittivity. It accounts for both static leakage and frequency-dependent dielectric loss, as follows:

$$G(\omega, D) = G_{dc}(D) + \omega\frac{\pi\varepsilon_0 Im\{\hat{\varepsilon}_r(\omega)\}}{\cosh^{-1}(\frac{D}{2 \cdot GMR})} \tag{13}$$

2.5 Characteristic impedance

The characteristic impedance, $Z_0(\omega, D)$ is a complex quantity that defines the ratio of voltage to current for a wave propagating along the transmission line. It is a fundamental parameter for analyzing signal integrity and power transmission (Pozar 2012).

$$Z_0(\omega, D) = \sqrt{\frac{R(\omega) + j\omega L(\omega, D)}{G(\omega, D) + j\omega C(\omega, D)}} \tag{14}$$

3. Modeling of transmission line and materials

In this study, a two-conductor transmission line embedded within a steel–concrete structure was modeled. The line consisted of a steel rebar and electrical wire that served as parallel conductors. The steel rebar had a radius of 12.5 mm, corresponding to a D25 rebar, which is commonly used in civil engineering applications. It was modeled as carbon steel with a DC electrical resistivity of 1.5×10^{-7} Ω·m at 20 °C and was assumed to be nonmagnetic. The electrical wire consisted of a copper conductor and insulation. The second conductor consisted of a bare copper wire with a radius of 1.05 mm, corresponding to American Wire Gauge (AWG) 16. The wire was encapsulated in a polyvinyl chloride (PVC) sheath with a thickness of 0.8 mm, resulting in an effective outer

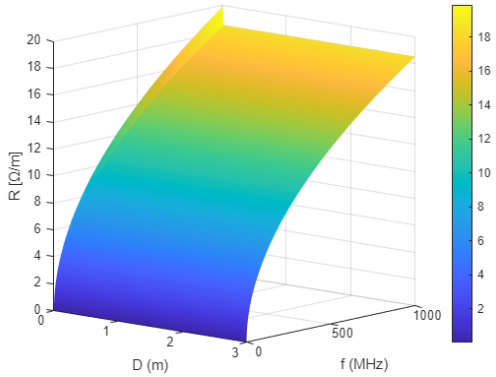

Fig. 1 3D surface plot of resistance vs. spacing and frequency

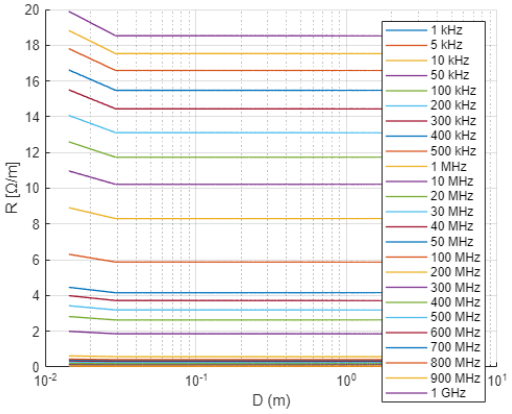

Fig. 2 Resistance vs. spacing at different frequencies

radius of 1.85 mm. Copper was modeled with a DC electrical resistivity of 1.68×10^{-8} Ω·m at 20 °C. The PVC sheath was non-conductive and served as an insulating dielectric medium. It was characterized by a relative permittivity of 3.4, typical for rigid PVC, and a loss tangent of 0.02 at 100 MHz.

The transmission line was embedded in a steel–concrete composite that served as a lossy dielectric medium with frequency-dependent electromagnetic characteristics. The relative permittivity of the concrete was swept from 5.0 to 10.0 to investigate the influence of the moisture content and aggregate composition. In addition, the dielectric loss tangent of concrete, which reflects the energy dissipation due to the polarization lag, varied between 0.02 and 0.1.

The minimum center-to-center spacing was defined as the point at which the PVC sheath of the electrical wire was in direct contact with the steel rebar, resulting in a minimum spacing of 14.35 mm. The spacing was swept from 14.35 to 3.0 m to evaluate the influence of conductor spacing.

To investigate the frequency-dependent behavior, the system was evaluated over a wide frequency range from 1 kHz to 1 GHz. This range encompasses the transition from quasi-static conditions, where the skin depth greatly exceeds the conductor radius and internal inductance plays a dominant role, to high radio frequencies, where the skin depth becomes much smaller than the conductor radius, and the transmission line exhibits an almost lossless behavior except for dielectric losses.

4. Results and analysis

4.1 Line parameters

The variations in resistance, inductance, capacitance, and conductance were investigated with respect to different conductor spacings, ranging from 14.35 mm (D_{min}) to 3 m (D_{max}), over a frequency range of 1 kHz to 1 GHz. A constant relative permittivity of 7.0 was assumed to represent the electromagnetic properties of dry concrete under low radio frequency conditions.

4.1.1 Resistance

At low frequencies (< 100 kHz), the resistance remained near the DC base line (≈ 0.005 Ω/m) and was essentially independent of the conductor spacing, because skin and proximity effects are negligible in this range, as shown in Fig. 1. As the frequency increased to the MHz range, the skin effect began to dominate, causing the resistance to increase in proportion to the frequency. Additionally, the influence of conductor spacing became more pronounced. When the conductors were placed close together at the minimum spacing, the proximity effect could amplify the resistance by up to 20% compared with that of widely separated conductors, with the amplification factor reaching approximately 1.2 when there was no separation margin. At 1 GHz, the combined effects of skin and proximity produced the highest resistance values, approximately 0.20 Ω/m, at the minimum spacing. In contrast, for conductor spacings greater than or equal to one meter, the resistance was governed solely by the skin effect and stabilized at approximately 0.16 Ω/m.

Notably, when conductors are placed close together, the magnetic fields generated by each conductor interact, thereby affecting the current distribution within each conductor. This interaction causes the current within the conductors to concentrate toward the surfaces facing away from the adjacent conductor (far-side surfaces). This phenomenon is known as the proximity effect. This causes uneven current distribution, reducing the effective cross-sectional area of the conductor available for current flow. A reduction in the effective cross-sectional area increases the resistance, resulting in a higher AC resistance.

At higher frequencies, the AC tends to concentrate near the surface of the conductors rather than being uniformly distributed throughout the conductor cross-section. This phenomenon is known as the skin effect. The skin effect becomes more pronounced as the frequency increases, significantly decreasing the effective cross-sectional area of the conductor available for current conduction. Consequently, this results in increased AC resistance at high frequencies. At low frequencies, the current distribution remains relatively uniform across the conductor cross-section. Therefore, reducing the conductor spacing has minimal additional impact on the resistance. However, at high frequencies, both the skin and proximity effects intensify simultaneously. Consequently, the current becomes confined to an even narrower region (specifically,

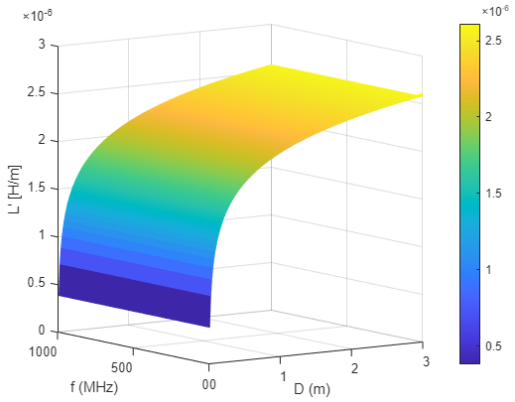

Fig. 3 3D surface plot of inductance vs. spacing and frequency

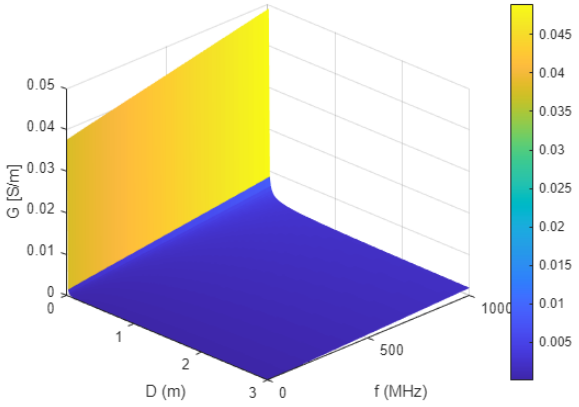

Fig. 4 3D surface plot of conductance vs. spacing and frequency

the conductor surfaces farthest from the neighboring conductor), sharply increasing the AC resistance as the spacing decreases, as shown in Fig. 2.

4.1.2 Inductance

At low frequencies (below approximately 100 kHz), the skin depth was much larger than the conductor radius. In this regime, the internal inductance remained close to its maximum value, and the total inductance remained nearly constant with the frequency, as shown in Fig. 3. In the mid-frequency range from approximately 1 to 100 MHz, the skin depth became smaller than the conductor radius. Consequently, the internal inductance decreased, leading to a noticeable drop in the total inductance, typically by 20%–50%, approaching the value determined purely by the external geometry of the conductors. At frequencies above 200 MHz, the energy storage within the conductor became negligible, and the internal inductance approached zero. Consequently, the total inductance converged to the external inductance, which depended only on the spacing between conductors. Beyond this point, the inductance exhibited no further variation with frequency.

The total inductance increased monotonically with the spacing owing to the logarithmic growth of the external inductance. At high frequencies, the slope was independent of frequency because the internal contribution was negligible. At low frequencies, the vertical offset of the inductance curves was larger by approximately 1.0×10^{-7} H/m owing to the internal component. In the DC-like regime, where the skin depth was significantly greater than the conductor radius, the total inductance was the sum of the external and internal components. In the high-frequency regime, where the skin depth was significantly smaller than the conductor radius, the total inductance was equal to that of the external component. In the transition region, the total inductance decreased smoothly with the frequency until the external term dominated.

Inductance is directly related to the magnetic field generated around the conductor when the current flows. As the spacing between the conductors increases, the magnetic flux linkage between the conductors expands, thus lengthening the magnetic field paths. This expanded field path increases the magnetic energy stored in the field, which directly increases the inductance. Conversely, when the conductor spacing decreases, the magnetic fields from each conductor tend to partially cancel each other out, reducing the total magnetic energy storage and thus lowering the inductance.

The inductance fundamentally depends on the conductor geometry and magnetic flux linkage, both of which are typically unaffected by the frequency. Under real-world conditions, the skin and proximity effects occur at very high frequencies, causing the current to concentrate on the conductor surface. This concentration of current at the surface of the conductor reduces the penetration depth of the magnetic field inside the conductor, slightly lowering the effective magnetic flux, and, therefore, slightly decreasing the inductance. However, this reduction is typically very small and is neglected in practical design considerations.

Inductance is highly sensitive to changes in conductor spacing but is generally insensitive to changes in frequency. However, at very high frequencies with a small conductor spacing, the inductance can experience a slight decrease owing to intensified proximity and skin effects. Inductance is predominantly determined by the physical geometry (spacing and arrangement of conductors), with spacing having the primary influence on inductance. Frequency typically has little effect on the inductance because the overall magnetic flux linkage remains relatively stable across a wide frequency range. However, at very high frequencies, the current is restricted to a thin surface layer of the conductor, which reduces magnetic flux penetration. This effect slightly decreases the inductance, which is particularly noticeable for closely spaced conductors.

4.1.3 Conductance

The DC leakage conductance increased significantly as the conductor spacing approached the minimum value owing to the reduced separation between the conductive surfaces. For near-contact spacing, the leakage conductance was capped by a geometry-based scaling factor and reached values on the order of 4×10^{-2} S/m, as shown in Fig. 4. In contrast, at wide separations such as 3 m, the conductance

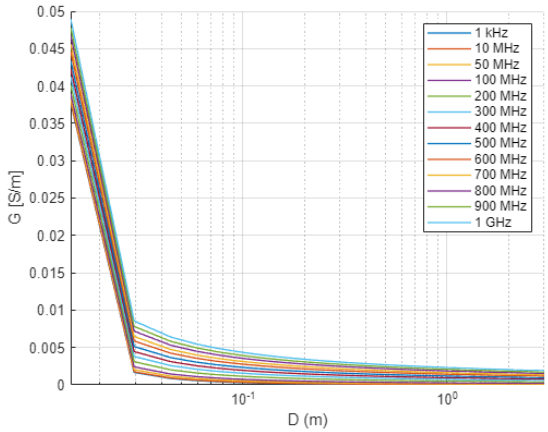

Fig. 5 Conductance vs. spacing at different frequencies

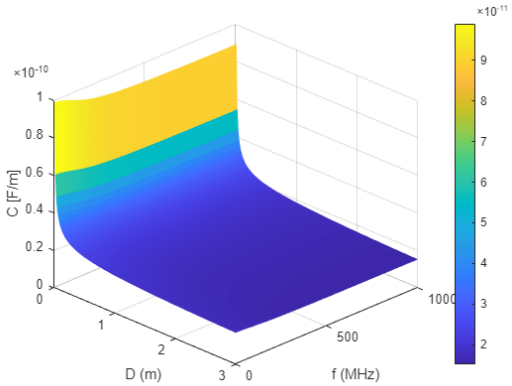

Fig. 6 3D surface plot of capacitance vs. spacing and frequency

dropped to approximately 1 × 10⁻⁶ S/m. Overall, the DC conductance spanned nearly five orders of magnitude as the spacing increased from near the contact to m.

Given a constant loss tangent, the dielectric loss component was directly proportional to the frequency. This term increased linearly across the operating range because the capacitance changed only slightly with the frequency. At 1 kHz, the dielectric-loss contribution was approximately 1.3 × 10⁻⁸ S/m, whereas at 1 GHz, it increased to about 1.1 × 10⁻² S/m. This resulted in a broad dynamic range for the dielectric-loss conductance component.

At low frequencies (≲ 10 MHz) and small conductor spacings, the total conductance was dominated by the DC leakage term. For example, at minimum spacing, the conductance was approximately 4 × 10⁻² S/m. Both the leakage and dielectric loss terms contributed comparably between approximately 10 and 100 MHz and at intermediate spacings. In this region, the conductance varied with both spacing and frequency. At high frequencies (≳ 200 MHz) or large spacings, leakage became negligible, and the total conductance was governed by dielectric loss. In this case, it increased linearly with frequency and decreased with spacing. For instance, at 1 GHz and 3 m spacing, the conductance was approximately 1 × 10⁻² S/m.

At a fixed frequency, the total conductance initially decreased sharply with increasing spacing owing to the reduced leakage and then asymptotically approached the dielectric-loss floor. For example, at 10 MHz, conductance decreased from about 4×10⁻² S/m at near-contact spacing to about 1×10⁻⁷ S/m at 3 m, then flattened near 1×10⁻⁶ S/m, as shown in Fig. 5. At a fixed spacing, the behavior depended on the dominance of the leakage term. For small spacing, the total conductance remained nearly constant until the dielectric-loss term exceeded the leakage component above approximately 100 MHz. For large spacings, the leakage was negligible, and the conductance increased linearly with the frequency, even at low frequencies. These trends provide a comprehensive understanding of the joint influence of spacing and frequency on the total conductance of the embedded transmission line.

Conductance in a transmission line is primarily associated with dielectric losses, which occur because of leakage currents flowing through the insulating material between the conductors. When conductors are placed close together, the electric field intensity in the insulating material between them increases significantly, resulting in greater dielectric losses and, therefore, increased conductance. Conversely, as the conductor spacing increases, the electric field intensity between the conductors weakens, reducing the leakage currents and thus decreasing the conductance.

Conductance is frequency-dependent, primarily owing to the dielectric loss properties of the insulating material. The complex permittivity of a dielectric material consists of a real part (related to energy storage) and an imaginary part (related to energy loss). At higher frequencies, the dielectric losses (associated with the imaginary component of the permittivity) increase, enhancing the leakage currents and thus increasing the conductance. Therefore, as the frequency increases, the effective conductance of the transmission line increases.

The narrow spacing intensifies the electric field, exacerbating the frequency-dependent dielectric losses at higher frequencies and resulting in a significantly elevated conductance. At larger spacings, the electric field intensity decreases, mitigating, but not eliminating, the frequency-dependent increase in the conductance. Thus, the frequency-induced increase in the conductance is relatively small when the conductor spacing is wide. Hence, the greatest increase in conductance occurs when conductors are closely spaced and the frequency is high because of the combined field intensity and high-frequency dielectric loss effects.

4.1.4 Capacitance

The capacitance decreased monotonically as the spacing between the conductors increased, following an inverse-logarithmic trend, as shown in Fig. 6. At the minimum spacing and low frequency, the capacitance reached a maximum value of approximately 1.0 × 10⁻¹⁰ F/m. In contrast, at a spacing of 3 m, the capacitance decreased to approximately 1.5 × 10⁻¹¹ F/m. This corresponded to a reduction of approximately a factor of seven, as the conductors were separated from the near contact by wide spacing.

The frequency dependence of capacitance is governed by Debye relaxation behavior. At low frequencies, well

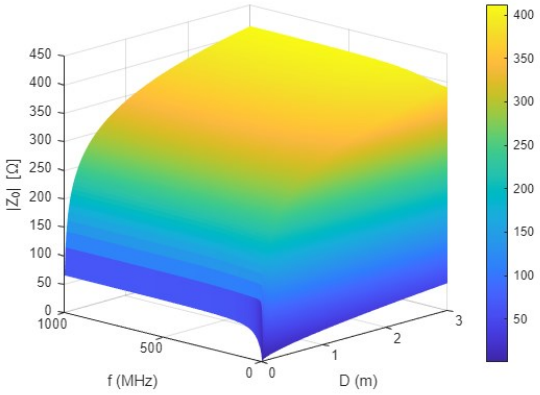

Fig. 7 3D surface plot of characteristic impedance vs. spacing and frequency

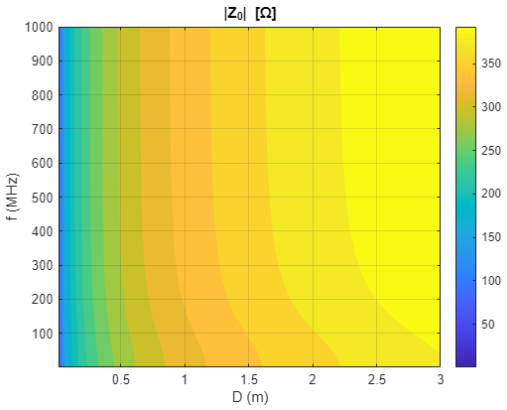

Fig. 8 2D contour plot of characteristic impedance vs. spacing and frequency

below the inverse of the dielectric relaxation time (approximately 160 MHz), the effective permittivity remained close to its static value, resulting in the maximum capacitance. At frequencies well above 160 MHz, the effective permittivity approached its high-frequency limit, which was approximately 90% of the static value.

Consequently, the capacitance decreased by approximately 10% in this frequency range. At any fixed spacing, the frequency-dependent variation in capacitance was relatively minor.

The combined influence of the spacing and frequency resulted in a gently sloping capacitance surface. At low frequencies and small spacing, the capacitance was approximately 1.0×10^{-10} F/m. At the same frequency but with large spacing, it decreased to about 1.5×10^{-11} F/m. At high frequencies, the capacitance for small spacing reduced to approximately 9.0×10^{-11} F/m, and for large spacing to about 1.35×10^{-11} F/m. Plotting these values yielded a capacitance surface that slopes steeply in the spacing direction, varying by a factor of seven, whereas the changes in the frequency direction were relatively mild, limited to approximately 10%.

Capacitance in transmission lines is directly related to the ability of the conductor arrangement to store electric energy in the electric field between the conductors. When the conductors are close to each other, the electric field intensity between them is strong. A strong electric field means that more electric charge can be stored per unit voltage difference, leading to a higher capacitance. Conversely, when the spacing between the conductors is increased, the electric field intensity weakens, reducing the ability to store charges per unit voltage and thereby decreasing the capacitance.

Ideally, capacitance is determined solely by geometric factors (such as spacing, conductor size, and dielectric permittivity) and thus does not significantly vary with frequency. However, actual dielectric materials exhibit frequency-dependent permittivities. At high frequencies, the real part of the permittivity may decrease slightly or vary owing to dielectric polarization mechanisms. This slight frequency-dependent variation in dielectric permittivity can cause minor changes in the capacitance at extremely high frequencies. Nevertheless, these changes are generally sufficiently small to be considered negligible in most practical transmission line designs.

The primary determinant of the capacitance is the geometry of the transmission line (spacing, conductor size, and dielectric thickness). Frequency-induced variations in capacitance occur only because dielectric materials change their permittivity slightly with increasing frequency.

Thus, even at high frequencies, geometric factors, particularly conductor spacing, dominate the capacitance determination. Only slight changes in the frequency response of the dielectric are observed under conditions of small spacing and extremely high frequencies.

4.2 Characteristic impedance

The characteristic impedance incorporates the combined effects of resistance, inductance, capacitance, and conductance. As shown in Fig. 7, the behavior of the characteristic impedance as a function of frequency and conductor spacing is summarized in Table 1.

At 10 kHz, the DC components dominated the losses. The characteristic impedance was primarily dictated by the ratio of the DC resistance to the leakage conductance, which exhibited an inverse relationship with the leakage conductance. As the spacing increased from 14.35 mm to 3 m, the leakage conductance decreased by five orders of magnitude, causing the impedance to increase from ~0.4 to ~70 Ω. At 10 MHz, the dielectric-loss term began to contribute, slightly constraining the increase in impedance caused by the reduced leakage. Nevertheless, the overall trend remained consistent and was characterized by a steep increase at small spacings and saturation behavior for spacings exceeding 0.1 m. At 1 GHz, both the resistance and conductance were negligible compared with those of the reactive components. Impedance followed the square root of the ratio of external inductance to capacitance and increased logarithmically with spacing, increasing from ~40 to ~300 Ω.

At minimum conductor spacing, the characteristic impedance remained nearly constant at approximately 0.4 Ω for frequencies below 100 kHz, indicating dominance of

Table 1 Frequency- and spacing-dependent behavior of characteristic impedance

Regime	Condition	Approximate behavior
Low-frequency, small spacing	Frequency $\lesssim$ 10 kHz, spacing $\approx$ minimum	Impedance $\approx$ 0.4 Ω
Low-frequency, large spacing	Frequency $\lesssim$ 10 kHz, spacing $\gg$ conductor radius	Impedance grows up to ~70 Ω
High-frequency, small spacing	Frequency $\gtrsim$ 200 MHz, spacing $\approx$ minimum	Impedance $\approx$ 40 Ω
High-frequency, large spacing	Frequency $\gtrsim$ 200 MHz, spacing $\gg$ conductor radius	Impedance rises to ~300 Ω

resistive and conductive effects. Between 100 kHz and 200 MHz, a sharp increase was observed as the line transitioned from resistive to reactive behavior, ultimately stabilizing at approximately 40 Ω. At moderate spacing (0.1 m), the impedance began in the range of a few ohms at low frequencies and increased steadily, reaching approximately 100 Ω at higher frequencies. For large spacing (1 m), the impedance began in the tens of ohms, increased significantly through the mid-frequency range, and plateaued at approximately 250 Ω as frequency increased further, as shown in Fig. 8.

Increasing the conductor spacing led to an increase in the characteristic impedance, whereas decreasing the spacing resulted in a decrease, as shown in Fig. 7. This is because the characteristic impedance is governed by the ratio of the inductance to the capacitance per unit length. As the conductor spacing increases, the capacitance decreases owing to a reduction in the electric field intensity between the conductors. Furthermore, the inductance increases because the magnetic field lines span a longer path, thereby enhancing the flux linkage. Both effects increase the inductance-to-capacitance ratio, thereby increasing the characteristic impedance. Conversely, as the spacing decreases, the capacitance increases owing to stronger electric fields, and the inductance decreases as the opposing magnetic fields from the two conductors tend to cancel. This reduces the inductance-to-capacitance ratio and characteristic impedance.

In ideal lossless transmission lines, the characteristic impedance is nearly constant across frequencies. However, in practice, lossy lines with slight frequency dependence are observed, particularly at high frequencies, owing to skin effects, proximity effects, and dielectric losses. The skin and proximity effects increase the resistance with frequency and slightly decrease the effective inductance owing to the limited magnetic field penetration. Dielectric losses (frequency-dependent conductance) increase with frequency, affecting the capacitance through the complex permittivity. These small variations in inductance, capacitance, resistance, and conductance cause slight frequency-dependent fluctuations in the characteristic impedance, which generally become more noticeable at very high frequencies (RF and microwave frequencies).

The conductor spacing primarily governs the characteristic impedance. Frequency introduces minor variations, especially at high frequencies and narrow spacing conditions, owing to intensified losses and effects such as skin and proximity effects. This is because geometric factors (conductor spacing and dimensions) dominate the determination of the characteristic impedance by significantly influencing the inductance and capacitance.

At high frequencies and narrow conductor spacing, the frequency-dependent losses become slightly more significant, causing subtle variations in the impedance value.

4.3 Limitations

This study considered the electrical properties of materials, such as conductivity, permittivity, and loss tangent, within limited predefined ranges. Effects of environmental conditions, including temperature changes and moisture fluctuations, which are known to alter these properties in actual structures, were excluded from the analysis. The investigation was purely theoretical, relying on established models without experimental validation. No comparison with measurement data from embedded transmission lines was performed.

Further research is needed to validate the findings through experimental studies on transmission lines embedded in steel–concrete composite structures. Studies should also examine the behavior of transmission lines under structural defects, including cracks, delamination, and corrosion, to assess their performance under realistic damage scenarios. In addition, since the electrical properties of concrete vary significantly with its composition, future work should address the influence of different concrete mix designs.

5. Conclusions

This study presents a computational analysis of the electromagnetic behavior of a transmission line embedded within a steel–concrete composite structure. The analysis focused on the key electrical parameters, including resistance, inductance, conductance, and capacitance, along with the characteristic impedance, across a wide frequency range from 1 kHz to 1 GHz and various conductor spacings ranging from 14.35 mm to 3 m.

The results showed that the dominant factors governing these parameters differ clearly. Inductance and capacitance were primarily affected by the geometric configuration. As the spacing between conductors increased, the inductance also increased, while the capacitance decreased following an inverse-logarithmic trend. The influence of frequency on these reactive components was relatively limited. At higher frequencies, inductance became nearly independent of frequency as internal inductive effects diminished, whereas capacitance exhibited only slight variation, approximately 10 percent, due to dielectric relaxation

In contrast, the resistance and conductance are strongly

dependent on both frequency and spacing. The resistance increases significantly with the frequency owing to the skin and proximity effects, with the latter being most pronounced at a narrow conductor spacing. The conductance shows high sensitivity to both variables, transitioning from a state dominated by DC leakage at low frequencies and small spacings to one governed by dielectric loss at high frequencies.

Ultimately, the characteristic impedance reflects the combined effects of these parameters, demonstrating a strong dependence on both conductor spacing and frequency. It transitions from a resistive-conductive behavior at low frequencies to a reactive (inductive-capacitive) behavior at high frequencies, with its magnitude increasing significantly with wider spacings and higher frequencies. These results offer a comprehensive understanding of the electromagnetic characteristics of embedded transmission lines, which is essential for the development and interpretation of structural health monitoring systems in complex steel–concrete environments. Furthermore, the findings of this study may provide valuable guidance for the design of transmission lines embedded in steel–concrete composite structures.

Acknowledgments

This work was supported by the National Research Foundation of Korea (NRF) grant funded by the Korea government (MSIT) (No. RS-2021-NR060085).

References

Aghda, S.F., GanjaliPour, K. and Nabiollahi, K. (2018), "Assessing the accuracy of TDR-based water leak detection system", *Results Phys*., **8**, 939-948.

Becker, D., Raddatz, L., Roussel, C. and Klonowski (2024), "Analysis methods for deformation detection using TLS and UAS data on the example of a landslide simulation", *Int. J. Geo-Eng*., **15**(9) 1-22.

Bogatin, E. (2004), *Signal Integrity: Simplified*, Prentice Hall Professional

Cataldo, A., De Benedetto, E., Cannazza, G., Masciullo, A., Giaquinto, N., D'Aucelli, G.M., Costantino, N., De Leo, A. and Miraglia, M. (2017), "Recent advances in the TDR-based leak detection system for pipeline inspection", *Measurement*, **98**, 347-354.

Cataldo, A., De Benedetto, E., Cannazza, G., Monti, G. and Demitri, C. (2016), "Accuracy improvement in the TDR-based localization of water leaks", *Results Phys*., **6**, 594-598.

Cole, R.H. (1977), "Time domain reflectometry", *Annual Rev. Phys. Chemistry*, **8**(1), 283-300.

Collin, R.E. (2007), *Foundations for Microwave Engineering*, John Wiley & Sons

Davis, J. and Annan, A. (1977), "Electromagnetic detection of soil moisture: Progress report I", *Canadian J. Remote Sensing*. **3**(1), 76-86.

Debye, P. (1913), "Reprinted 1954 in collected papers of Peter JW Debye Interscience, New York", *Ver. Deut. Phys. Gesell*, **15**, 777.

Dowell, P. (1966), "Effects of eddy currents in transformer windings", *Proceedings of the Institution of electrical Engineers*.

Farrington, S.P. and Sargand, S.M. (2006), "Advanced processing of time domain reflectometry for improved slope stability monitoring", *GeoCongress 2006: Geotechnical Engineering in the Information Technology Age. 2006*. 1-6.

Gnerlich, H.R. (1989). "Cable testing and cable fault locating with minimum risk to good cable", *Conference on Electrical Insulation and Dielectric Phenomena*.

Grigsby, L.L. (2007), *Electric Power Generation, Transmission, and Distribution*, CRC Press.

Islam, I., Ahmed, W. and Khattak, S.A. (2024). "Investigating the role of geological strength index and susceptible zones in landslide triggering mechanisms from Chukyatan-Kumrat road, Dir Upper, Pakistan", *Int. J. Geo-Eng*., **16**(10) 1-23.

Joseph, S.D., Huang, Y. and Hsu, S.S. (2020), "Transmission lines-based impedance matching technique for broadband rectifier", *IEEE Access*, **9**, 4665-4672.

Kalaga, S. and Yenumula, P. (2016), *Design of Electrical Transmission Lines: Structures and Foundations*, CRC Press

Kumar, A. (2020), "Time-domain reflectometry–based real-time slope stability monitoring in opencast mines: A review", *Noise Vib. Worldwide*. 0957456520924812.

Lee, D., Jeong, S., Han, W., Kim, J., Lee, J.-S. and Yu, J.-D. (2023a), "Application of electromagnetic waves for evaluating the integrity of model pile", *Smart Geotech. Smart Soc.*, CRC Press, 2023. 1399-1402.

Lee, D., Kim, D.-J., Kim, J., Lee, J.-S. and Kim, S.Y. (2024a), "A study on transmission line configuration for structural health monitoring using electromagnetic waves", *Smart Struct. Syst*., **34**(1), 1.

Lee, D., Kim, D.-J., Lee, J.-S., Tutumluer, E. and Byun, Y.-H. (2024b), "Evaluation of electrical resistivity of cement-based materials using time domain reflectometry", *Measurement*, **236**, 115166.

Lee, D., Lee, J.-S., Byun, Y.-H. and Kim, S.Y. (2023b), "Application of optimized time domain reflectometry probe for estimating contaminants in saline soil", *Geomech. Eng*., **33**(3), 291-299.

Lee, D., Lee, J.-S., Ju, Y.K. and Byun, Y.-H. (2024c), "Advanced electromagnetic wave-based method for characterizing defects in cement-based structures using time domain reflectometry", *Comput. Concrete*. **33**(5), 621-630.

Lee, D., Lee, J.-S., Yu, J.-D. and Park, J. (2025), "Experimental simulation for pile integrity: Electromagnetic assessment and pore topology analyses", *Case Studies Construct. Mater*., **22**, e04108.

Lee, D., Yoo, Y., Lee, J.-S. and Byun, Y.-H. (2024d), "Characterization of cement–slime mixture using time domain reflectometry", *Measurement*, **236**, 115071.

Lee, D., Yu, J.-D., Jeong, S., Park, G. and Lee, J.-S. (2024e), "Non-destructive method for evaluating local integrity of model piles using electromagnetic waves", *NDT & E Int*., **141** 102999.

Lee, J.-S. and Yu, J.-D. (2019), "Non-destructive method for evaluating grouted ratio of soil nail using electromagnetic wave", *J. Nondestruct. Evaluation*, **38**, 1-15.

Lee, J.-S. and Yu, J.-D. (2024), "Nondestructive evaluation of grout defect in rock bolt using electromagnetic waves", *Develop. Built Environ.*, **17**, 100365.

Lee, J.-S., Hong, W.-T., Park, K., Hong, S.-S., Lee, S.-H. and Byun, Y.-H. (2018), "Evaluation of water content in an active layer using penetration-type time domain reflectometry", *Appl. Sci*., **8**(6), 935.

Lee, J.-S., Lee, D., Kim, Y., Zi, G. and Yu, J.-D. (2023c), "Smart monitoring system using electromagnetic waves to evaluate the integrity of reinforced concrete structural elements", *Comput. Concrete*, **31**(4), 293-306.

Lee, J.-S., Song, J.U., Hong, W.-T. and Yu, J.-D. (2018), "Application of time domain reflectometer for detecting necking defects in bored piles", *NDT & E Int*., **100**, 132-141.
Lin, C.-P. (2009). "Geotechnical Sensing By TDR: A Slope Monitoring System Example", *ISOPE International Ocean and Polar Engineering Conference*.
Noborio, K. (2001), "Measurement of soil water content and electrical conductivity by time domain reflectometry: a review", *Comput. Electronics Agriculture*, **31**(3), 213-237.
Nur, A.-S., Nam, B.-H., Choi, S. and Kim, Y.-J. (2024), "Monitoring of ground subsidence using PS-InSAR technique in the Southeast Texas (SETX) Region", *Int. J. Geo-Eng*., **15**(13) 1-13.
O'connor, K.M. and Dowding, C.H. (2021), *Geomeasurements by Pulsing TDR Cables and Probes*, CRC Press
Park, G., Kim, N., Kang, S., Kim, S.Y., Yoo, C. and Lee, J.-S. (2023), "Instrumented dynamic cone penetrometer incorporated with time domain reflectometry", *Measurement*, **206**, 112337.
Park, K., Kim, Y.-J., Chen, J. and Nam, B.-H. (2024), "InSAR-based investigation of ground subsidence due to excavation: a case study of Incheon City, South Korea", *Int. J. Geo-Eng*., **15**(26), 1-10.
Pastuszka, T., Krzyszczak, J., Sławiński, C. and Lamorski, K. (2014), "Effect of time-domain reflectometry probe location on soil moisture measurement during wetting and drying processes", *Measurement*, **49**, 182-186.
Paul, C.R. (2007), *Analysis of Multiconductor Transmission Lines*, John Wiley & Sons
Pozar, D.M. (2012), "Microwave engineering", *University of Massachusetts at Amherst, John Wiley & Sons, Inc*. 26-30.
Robinson, D.A., Jones, S.B., Wraith, J.M., Or, D. and Friedman, S.P. (2003), "A review of advances in dielectric and electrical conductivity measurement in soils using time domain reflectometry", *Vadose Zone J*., **2**(4), 444-475.
van Rensburg, P.A.J., Sibanda, M.P. and Ferreira, H.C. (2014), "Integrated impedance-matching coupler for smart building and other power-line communications applications", *IEEE Transact. Power Delivery*, **30**(2), 949-956.
Wahab, N.S., K, N.W., Abdullah, N.H., Ibrahim, A., Majid, M.R., Ismail, B.N., Ramli, R. and Mansor, S. (2016). "Potential of time domain reflectometry as early warning system in slope stability monitoring project: A review", *AIP Conference Proceedings*.
Yu, J.-D. and Lee, J.-S. (2020), "Smart sensing using electromagnetic waves for inspection of defects in rock bolts", *Sensors*, **20**(10), 2821.
Yu, J.-D., Kim, K.-H. and Lee, J.-S. (2018), "Nondestructive health monitoring of soil nails using electromagnetic waves", *Canadian Geotech. J.*, **55**(1), 79-89.
Yu, J.-D., Kim, S.Y. and Lee, J.-S. (2020a), "Variations in velocity and sensitivity of electromagnetic waves in transmission lines configured in model piles with necking defects containing soils", *Sensors*, **20**(22), 6541.
Yu, J.-D., Lee, J.-S. and Yoon, H.-K. (2020b), "Circular time-domain reflectometry system for monitoring bridge scour depth", *Marine Georesources Geotechnol.*, **38**(3), 312-321.